Bulletin of the Seismological Society of America. Vol. 61, No. 1, pp. 177–194. February, 1971

A TWO-DIMENSIONAL MOVING DISLOCATION MODEL FOR A STRIKE-SLIP FAULT

By David M. Boore*, Keiiti Aki and Terry Todd

ABSTRACT

For a propagating, vertical, strike-slip fault whose breakage extends to the Earth's surface, previous studies by Aki (1968) and Haskell (1969) have suggested that the near-field motions may be similar to those from uniformly-gliding-edge dislocations. The theory of these dislocations in uniform motion leads to a simple, convenient relation between the perpendicular and parallel components of motion at the fault's surface. A number of examples are considered in order to illustrate this relation between the horizontal components. In general, step-function-like parallel motions result in pulse-like perpendicular displacements. For a given parallel displacement, the amplitude of the pulse depends in a concise manner on ratios of the rupture to shear-wave velocity, and on shear- to compressional-wave velocity. Increasing either of these ratios leads to an increased pulse-amplitude. The dislocation model is applied to the near-field observations of the Parkfield earthquake. The resulting estimate of the total fault offset is within the range of those based on the more detailed models of Aki (1968) and Haskell (1969).

Introduction

The effort now being made to instrument active faults will provide seismologists with excellent near-field seismic data. In order to interpret this data, attention must be given to the calculation of the near-field motion for various fault models. This, in general, is a very complex problem. Aki (1968) and Haskell (1969) have studied the displacements near a unilaterally-propagating, vertical strike-slip fault in an homogeneous medium, taking the free surface into account in an approximate way. Even in this simplified fault model a lengthy numerical integration of the Green's function over the fault surface was necessary. The above authors noted, however, that for a site near the fault the seismic motion was predominantly governed by the relative motion of the two sides of the fault near the site, not by the total fault length and width. This implies that the much simpler two-dimensional solution for the elastic field of a uniformly-moving dislocation might be of some use, both in interpreting measurements and in predicting the effects of variations in Poisson's ratio and rupture velocity. This idea will be explored in this paper.

Model of a Propagating Strike-Slip Fault

In the studies of Haskell and Aki, the fault was assumed to be in an infinite medium. The fault was specified by the time-spatial variation of the relative motion across the fault surfaces and was confined to a rectangular region. With reference to Figure 1, the fault was assumed to start at the left side and propagate uniformly to the right, stopping at the right-hand edge. The strike-slip nature of the fault was specified by allowing a discontinuity in only the u-displacement. The effect of the free surface was approximated by mirroring the fault about the x-y plane. Aki showed that if the condition

* Now at National Center for Earthquake Research, U. S. Geological Survey, Menlo Park, California 94025.

$H/\sqrt{\lambda r} \gg \sqrt{\pi/2}$ was met, where λ is the compressional wavelength and r is the distance to the fault, the width H of the fault was not important to the total motion. Furthermore, he found that for a station some distance from either end, the starting and stopping effects (Savage, 1965) did not contribute to the motion; in essence, these are far-field terms and are small compared to the near-field terms governed by the dislocation motion near the fault. Thus we can approximate, for recording sites near a fault and

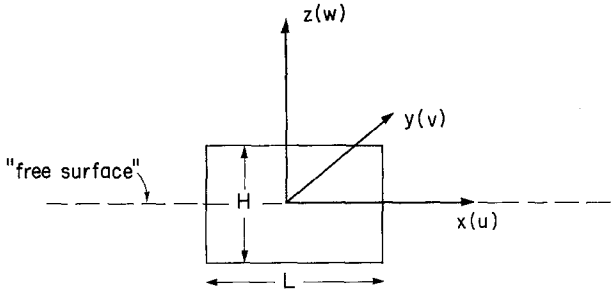

FIG. 1. The fault model used by Aki (1968) and Haskell (1969). The relative displacement across both sides of the fault is a function of time and position. The z-direction is considered vertical and u, v, w are components of displacement.

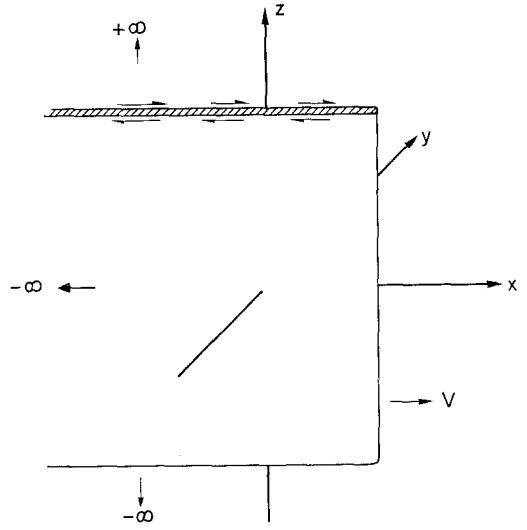

FIG. 2. A discrete gliding-edge dislocation representation, as seen in the stationary frame at some instant of time, of the fault model shown in Figure 1. Most of the dislocation models in this paper are not discrete, but have a displacement discontinuity which is a function of position along the moving dislocation.

removed from its ends, a horizontally-propagating, vertical strike-slip fault by a gliding-edge dislocation moving at uniform velocity, with the dislocation line parallel to the z-axis and the Burger's vector (Weertman and Weertman, 1964) in the x-direction (Figure 2). For the purposes of this paper we will assume that the dislocation across the fault surface is a specified function of time. We are not attempting to solve the more interesting and difficult problem of the dynamics of stress relaxation, which must depend in a complicated way on pre-existing stresses and elastic as well as nonelastic properties of the material.

The mathematical description of our problem is straightforward. Consider two half-

spaces of linear, isotropic, homogeneous material joined by a plane ($y = 0$) along which the fault propagates. We assume here that all nonelastic processes take place within a narrow zone between the two fault surfaces (see Haskell, 1964, for a discussion of this idealization). With the assumption that the z-component of displacement is zero ($w = 0$), the following equations describe the motion

$$\nabla^2\phi = \frac{1}{\alpha^2}\frac{\partial^2\phi}{\partial t^2}$$

$$\nabla^2\psi = \frac{1}{\beta^2}\frac{\partial^2\psi}{\partial t^2} \tag{1}$$

where

$$u = \frac{\partial\phi}{\partial x} - \frac{\partial\psi}{\partial y}, \qquad v = \frac{\partial\phi}{\partial y} + \frac{\partial\psi}{\partial x} \quad \text{and} \quad \alpha, \beta$$

are the compressional and shear velocities. Following Fung (1965), we change coordinates into a moving frame by the transformation

$$x' = x - Vt$$

$$y' = y$$

$$t' = t \tag{2}$$

where V is the rupture (propagation) velocity of the fault.

With the further assumption that in the moving frame there are no transient motions (i.e., the dislocation has been moving at constant velocity V since $t = -\infty$), we can replace time derivatives by

$$\frac{\partial}{\partial t} = -V\frac{\partial}{\partial x'}. \tag{3}$$

Doing this and dropping primes, with the understanding that we now consider quantities in the moving coordinate system, gives

$$\gamma_1^2\frac{\partial^2\psi}{\partial x^2} + \frac{\partial^2\psi}{\partial y^2} = 0$$

$$\gamma_2^2\frac{\partial^2\phi}{\partial x^2} + \frac{\partial^2\phi}{\partial y^2} = 0 \tag{4}$$

where

$$\gamma_1^2 = 1 - M_1^2, \gamma_2^2 = 1 - M_2^2 \quad \text{and} \quad M_1, M_2,$$

the Mach numbers, are defined by

$$M_1 = V/\beta$$

$$M_2 = V/\alpha.$$

We consider here subsonic motion only, that is, $M_1 < 1$. Then γ_1, γ_2 are real and equation (4) is elliptic.

Along the boundary between the half-species, we specify a discontinuity in the parallel component of motion

$$\Delta u(x, 0) = u(x, +0) - u(x, -0) \equiv u^+ - u^-. \tag{5}$$

With the further assumption $u^+ = -u^-$, each half-space can be treated separately. Another condition is that the perpendicular component of stress, σ_{yy}, vanish across the fault surface. The need for this condition can be argued from symmetry and the need for no unbalanced forces to remain after integration of the forces on a loop around the dislocation. As a check on the consistency of the solution, the perpendicular displacement v and the shear stress σ_{xy} should be continuous across the fault plane when we join the solutions in each half-space.

Solution

Several equivalent forms of the solution are useful. The standard separation-of-variables, Fourier transform approach gives

$$u(x, y) = \operatorname{sgn}(y) \int_{-\infty}^{\infty} \{e^{-|k|\gamma_2|y|} - \chi^2 e^{-|k|\gamma_1|y|}\} f(k) e^{ikx}\, dk \tag{6a}$$

$$v(x, y) = \int_{-\infty}^{\infty} \left\{\gamma_2 e^{-|k|\gamma_2|y|} - \frac{\chi^2}{\gamma_1} e^{-|k|\gamma_1|y|}\right\} e^{i(\pi/2) \operatorname{sgn} k} f(k) e^{ikx}\, dk \tag{6b}$$

where $\chi^2 = 1 - \frac{1}{2}M_1^2$ and $f(k)$ is related to the Fourier transform $U^+(k)$ of $u^+(x)$ by

$$f(k) = \frac{U^+(k)}{2\pi(1 - \chi^2)}. \tag{6c}$$

Note that, if we are interested in the displacements along the fault, then the perpendicular component has an antisymmetric relation to the parallel component, and furthermore, the influence of the velocities on the perpendicular motion for any given form of the dislocation is given entirely by the factor

$$\text{AMP} = \frac{\chi^2 - \gamma_1\gamma_2}{\gamma_1(1 - \chi^2)}. \tag{7}$$

We will discuss the behavior of this function later.

We have already noted the elliptic character of the equations of motion. Because of this and the two-dimensionality, we should expect complex variable analysis to be intimately related to the solutions. Eshelby (1949) showed, in fact, that, if we break the motion into distortional and dilatational parts u_1, v_1 and u_2, v_2 [as is implied in equations (1)], the following relations exist

$$u_1 = \operatorname{Im} P(x + i\gamma_1 y), \qquad \gamma_1 v_1 = \operatorname{Re} P(x + i\gamma_1 y)$$

$$\gamma_2 u_2 = \operatorname{Im} Q(x + i\gamma_2 y), \qquad v_2 = \operatorname{Re} Q(x + i\gamma_2 y) \tag{8}$$

where P and Q are analytic functions in the half-plane of interest. These relations are convenient if we have one component of displacement [typically $u(x, y)$] and need the other. The forms above, however, do not guarantee that the interface conditions are met. These conditions imply relations between P and Q. Restricting our attention to the upper half-space $y \geqq 0$ and with $P(x, y) = P_R(x, y) + iP_I(x, y)$ [and similarly for $Q(x, y)$],

$$P_I(x, 0) + \frac{1}{\gamma_2} Q_I(x, 0) = u(x, +0) \equiv u^+. \tag{9}$$

In addition, the stress condition $\sigma_{yy} = 0$ becomes

$$\alpha^2 \left\{ \frac{\partial P_R}{\partial(\gamma_1 y)} + \gamma_2 \frac{\partial Q_R}{\partial(\gamma_2 y)} \right\}_{y=0} + (\alpha^2 - 2\beta^2) \left\{ \frac{\partial P_I}{\partial x} + \frac{1}{\gamma_2} \frac{\partial Q_I}{\partial x} \right\}_{y=0} = 0. \tag{10a}$$

Using the Cauchy-Riemann equations, relating the real and imaginary parts of an analytic function, we find

$$\frac{\partial}{\partial x} \left\{ P_I + \frac{\chi^2}{\gamma_2} Q_I \right\} = 0 \tag{10b}$$

or, to within an arbitrary constant that represents a rigid body displacement,

$$P_I(x, 0) + \frac{\chi^2}{\gamma_2} Q_I(x, 0) = 0. \tag{10c}$$

Solving (9) and (10c) gives

$$Q_I(x, 0) = \frac{\gamma_2}{(1 - \chi^2)} u^+(x) \tag{11}$$

and

$$P_I(x, 0) = \frac{-\chi^2}{(1 - \chi^2)} u^+(x). \tag{12}$$

Knowing the imaginary parts, we can derive the real parts by using a theorem given in Titchmarsh (1948) which states that the real part and the negative of the imaginary part of a suitably integrable, analytic function which is regular in the upper half-plane are Hilbert transform pairs along the real axis. Thus, e.g.,

$$P_R(x) = \frac{1}{\pi} \mathscr{J}_{-\infty}^{\infty} \frac{P_I(t)}{t - x} dt \tag{13}$$

where $\mathscr{J}$ stands for the Cauchy principal value of the integral. (Relations of this type, often referred to as Kramers-Krönig equations, have been used in another context in seismology in the studies by Futterman (1962) and Lamb (1962) of the dispersion accompanying absorption of waves.) We have glossed over the condition on integrability. For most of the functions considered here, this condition is met. When it is not (as in a

discrete dislocation) we do not use this approach. With the values of P and Q along the (real) x-axis we could extend the results for $y \geqq 0$ by analytic continuation. Our main interest, however, is in the displacements very close to the fault, for it is here that our neglect of the fault width is most valid. In that case the equations above give

$$v(x, +0) = -\frac{(\chi^2 - \gamma_1\gamma_2)}{\gamma_1(1 - \chi^2)} \frac{1}{\pi} \mathcal{P}\int_{-\infty}^{\infty} \frac{u^+}{t - x}\, dt. \tag{14}$$

We note that the factor containing the velocities is the same as in (7). We could, in fact, have derived (14) directly from (6b) by using the convolution theorem. The usefulness of (14) lies in the existence of tables of Hilbert transforms for a wide variety of functions (e.g., Erdélyi, 1954).

As seen in (14), the perpendicular displacement along the fault depends both on the

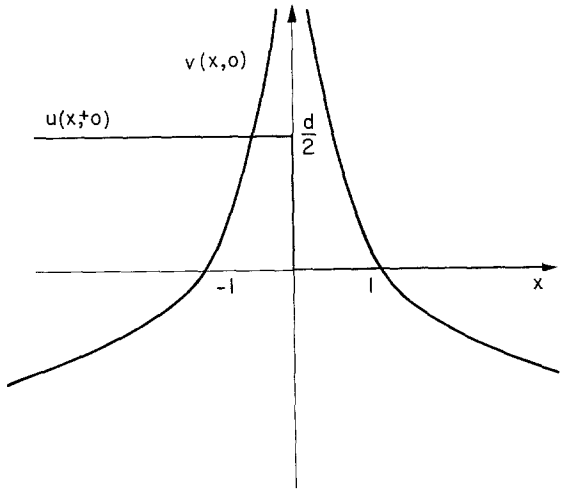

FIG. 3. Components of motion along the fault for discrete gliding-edge dislocation. The perpendicular displacement is schematic. In this and all other figures, the sense of motion is appropriate for a right-lateral fault.

velocity ratios and the dislocation across the fault surface. The influence of these two factors will be studied separately, starting with the form of the dislocation. In all of the examples to follow, the sign of the dislocation will be chosen so as to model a right-lateral fault, and the maximum total amplitude of the dislocation will be d.

DISCRETE DISLOCATION

The simplest and most obvious dislocation function is a simple step discontinuity in the parallel component of displacement. This corresponds to the classical discrete-edge dislocation. Following Eshelby (1949), we can easily show from equation (6a) that for a fault motion of total offset d

$$u(x, y) = \frac{d}{2\pi(1 - \chi^2)} \left\{ \tan^{-1} \frac{\gamma_2 y}{x} - \chi^2 \tan^{-1} \frac{\gamma_1 y}{x} \right\}. \tag{15a}$$

(Note that since the total dislocation, d, is accounted for by equal but opposite motion of each side of the fault surface, the maximum offset on a given side of the fault is

$d/2$.) Furthermore, using the relation

$$\log (x + iy) = \log [x^2 + y^2]^{1/2} + i \tan^{-1} (y/x)$$

and equations (8) we can write down the perpendicular displacement

$$v(x, y) = \frac{-d}{2\pi(1 - \chi^2)} \left\{ \frac{\chi^2}{\gamma_1} \log [x^2 + \gamma_1^2 y^2]^{1/2} - \gamma_2 \log [x^2 + \gamma_2^2 y^2]^{1/2} \right\}. \quad (15b)$$

The components of motion along the fault surface are sketched in Figure 3. We note that the perpendicular component exhibits an infinite peak in displacement at the origin and that it tends to $-\infty$ for $|x| \to \infty$. As we will illustrate later, the peak at the origin is due to the discontinuity in the parallel component, whereas the behavior of

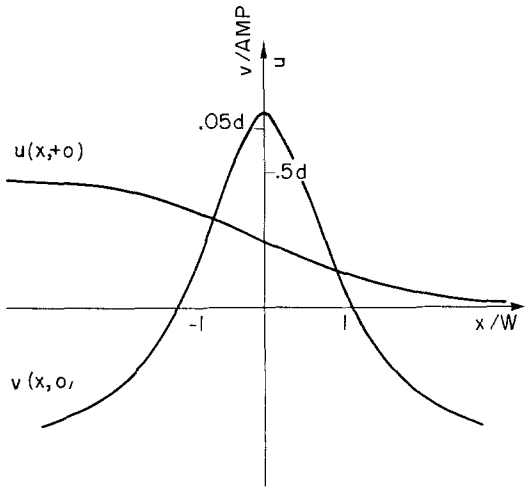

FIG. 4. Components of motion along the fault for a smoothed-out-edge dislocation, as given by equations (17). For purposes of illustration, a constant displacement has been added such that $v(1, 0) = 0$.

the displacement far from the origin is governed by the finite offset in the parallel component. As it is, the perpendicular displacement is obviously not useful quantitatively, although it does predict the sense-of-direction of the motion. We thus study a series of smoothed-out dislocations which might be more useful in quantitative comparisons with observations.

SMEARED-OUT DISLOCATIONS

In order to smooth the discrete jump at the origin, we consider first a dislocation given by

$$u^+(x) = \frac{d}{2\pi} \tan^{-1} \frac{W}{x} \quad (16)$$

where W is a parameter controlling the distance over which the final offset is reached. As $W \to 0$, $u^+ \to$ a step function equivalent to that discussed in the section above. We

can use the previous results and write down the solution here almost by inspection. It is

$$u(x, y) = \frac{d \operatorname{sgn} y}{2\pi(1 - \chi^2)} \left\{ \tan^{-1} \frac{\gamma_2 |y| + W}{x} - \chi^2 \tan^{-1} \frac{\gamma_1 |y| + W}{x} \right\} \tag{17a}$$

$$v(x, y) = \frac{-d}{2\pi(1 - \chi^2)} \left\{ \frac{\chi^2}{\gamma_1} \log [x^2 + (\gamma_1 |y| + W)^2]^{1/2} - \gamma_2 \log [x^2 + (\gamma_2 |y| + W)^2]^{1/2} \right\}. \tag{17b}$$

The solution along the fault surface is sketched in Figure 4. We have eliminated the infinite pulse at the origin, but the logarithmic divergence for $|x| \to \infty$ still exists.

This divergence is a common feature of two-dimensional, steady-state solutions

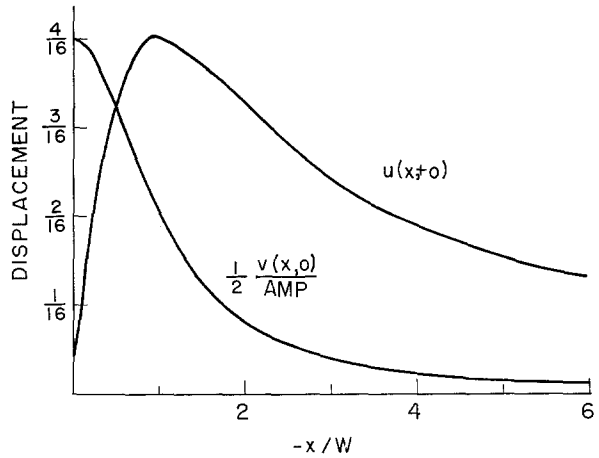

FIG. 5. Components of motion, along the fault surface, as given by equations (19). The parallel component is antisymmetric and the perpendicular component is symmetric about $x = 0$. The units of displacement in this and the following figures is d, the total dislocation.

(Fung, 1965, p. 264) and is obviously unphysical. It seems reasonable that it could be eliminated by not requiring a constant offset at $|x| = \infty$, allowing instead the dislocation to approach zero far from the tip of the fault. This is somewhat justified by the physical model we are attempting to model by two-dimensional dislocations; the dislocation along the real fault approaches zero for x large. A convenient function for the dislocation is

$$u^+(x) = -\frac{d}{2}\left[\frac{(x/W)}{(x/W)^2 + 1}\right] \tag{18}$$

as it is easy to find $v(x, y)$, and it also approximates the form of the dislocation found by Aki (1968). It does have the rather unphysical feature that the surface area over which the faulting has taken place remains constant with time, rather than starting from a point and sweeping out an ever-increasing area. Since the function in (18) is in the moving frame, this means the dislocation established across the fault at any point must relax in time such that the dislocation surface remains constant. The decay with dis-

tance of the dislocation and the constancy of the area of dislocation must be retained if logarithmic divergences for large x are to be avoided and if the assumption of a steady-state solution in the moving frame is to be used. It must be remembered, however, that our basic approximation of a three-dimensional faulting process by a two-dimensional one precludes an accurate description of the fault, and, in this light, the undesirable feature above is not crucial. What we desire is to predict certain features of the displacement which, within the limited bandwidth of the observations, are useful approximations of more realistic (and more complicated) fault models.

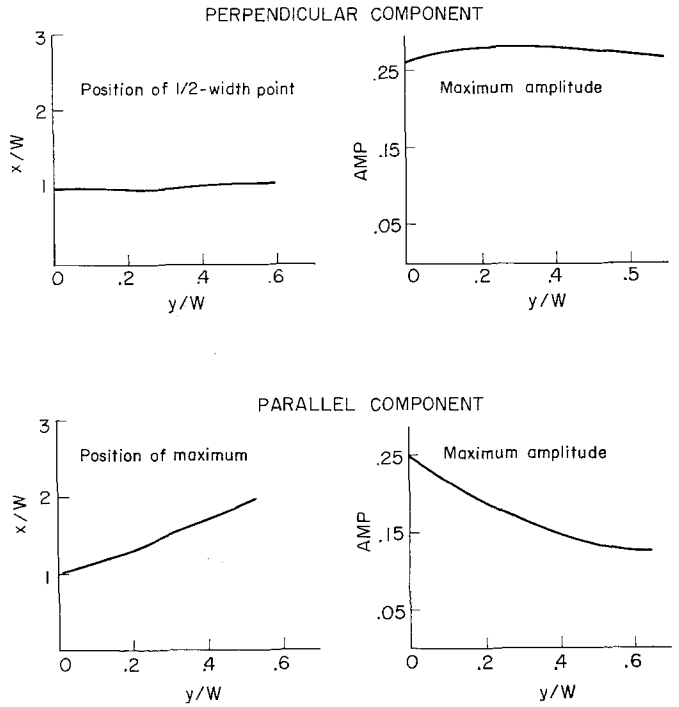

FIG. 6. The behavior of the motions given by (19) as a function of distance from the fault; in this example $V = 2.2$, $\beta = 3.5$, and $\alpha = 6.0$ km/sec.

The solution in this case is

$$u(x, y) = \frac{-dW}{2(1 - \chi^2)} \left\{ \frac{x}{x^2 + (\gamma_2 |y| + W)^2} - \chi^2 \frac{x}{x^2 + (\gamma_1 |y| + W)^2} \right\} \operatorname{sgn}(y) \quad (19a)$$

$$v(x, y) = \frac{dW}{2(1 - \chi^2)} \left\{ \chi^2 \frac{(\gamma_1 |y| + W)}{\gamma_1 [x^2 + (\gamma_1 |y| + W)^2]} - \gamma_2 \frac{(\gamma_2 |y| + W)}{[x^2 + (\gamma_2 |y| + W)^2]} \right\}. \quad (19b)$$

These displacements are plotted in Figure 5 for $y = 0$. Interesting features of the solution for other values of y are that the rise-distance in the parallel displacement increases with y, and, along $x = 0$, the peak in the perpendicular displacement occurs at

$$y/W = \frac{\chi/\gamma_2 - 1}{\gamma_1 - \chi} \quad (20)$$

and not at the fault surface. These features are shown in Figure 6 for a particular choice of the velocities.

Returning to Figure 5, we see that the divergence at infinity has been removed, as has the infinite pulse at the origin. The function considered does not, however, seem to offer enough flexibility of form for application to observations. In particular, a discrete dislocation cannot be recovered from the function; rather, in the limit $W \to 0$ the dislocation becomes a doublet, similar to the derivative of a δ function. Thus, we consider still another form for the dislocation.

The form we choose is

$$u^+(x) = -A(a, b)e^{-ab\xi}\{1 - e^{-\xi}\} \operatorname{sgn} x \tag{21}$$

where $\xi = |x|/a$ and $A(a, b)$ is chosen such that the peak to peak amplitude is $d/2$. The maximum value occurs at

$$\xi = \log\left[\frac{ab + 1}{ab}\right] \tag{22}$$

and gives

$$A(a, b) = \frac{d}{4}(1 + ab)\left(\frac{1 + ab}{ab}\right)^{ab}. \tag{23}$$

Restricting our attention to the fault surface, $y = 0$, we find that the perpendicular displacement from equation (14) and the table of Hilbert transforms given in Erdélyi (1954) is

$$\begin{aligned} v(x, 0) = {} & \frac{A(a, b)}{\pi}\frac{(\chi^2 - \gamma_1\gamma_2)}{\gamma_1(1 - \chi^2)}\{e^{-(ab+1)\xi}\bar{E}_i[(ab + 1)\xi] \\ & + e^{(ab+1)\xi}E_i[-(ab + 1)\xi] - e^{-ab\xi}\bar{E}_i[ab\xi] \\ & - e^{ab\xi}E_i[-ab\xi]\} \end{aligned} \tag{24}$$

where E_i, $\bar{E}_i$ are exponential integrals as defined in Erdélyi (1954). In the limit $\xi \to 0$ the displacement becomes

$$v(0, 0) = \frac{2A(a, b)}{\pi}\frac{(\chi^2 - \gamma_1\gamma_2)}{\gamma_1(1 - \chi^2)}\log\frac{ab + 1}{ab} \tag{25}$$

and for large x, $v(x, 0) \to 0$. Expansions given in Gautschi and Cahill (1965), were used to derive these limits. Plots of $u(x, 0)$ and $v(x, 0)$/AMP, calculated from equations (21) and (24) with the help of the tables in Gautschi and Cahill, are given in Figure 7 for a range of ab values. The general effect of decreasing ab is to produce a larger perpendicular displacement. In the limit $ab \to 0$, we either have a parallel component (A) with a discrete jump at $x = 0$ and no residual at infinity, or (B) a finite residual at infinity but a smooth dependence near the origin, depending on whether a or b approaches zero (e.g., the effect of $a \to 0$ is shown in Figure 8). In either case, our previous examples lead us to expect that the *total* perpendicular displacement is infinite;

in case (A), above, this infinity should occur closer to the origin, as a spike, than in case (B) where the perpendicular displacement will diverge logarithmically as $|x| \to \infty$. If we keep in mind the ambiguity of the displacements to within rigid body motions, we can see that the results in Figure 7 satisfy these expectations.

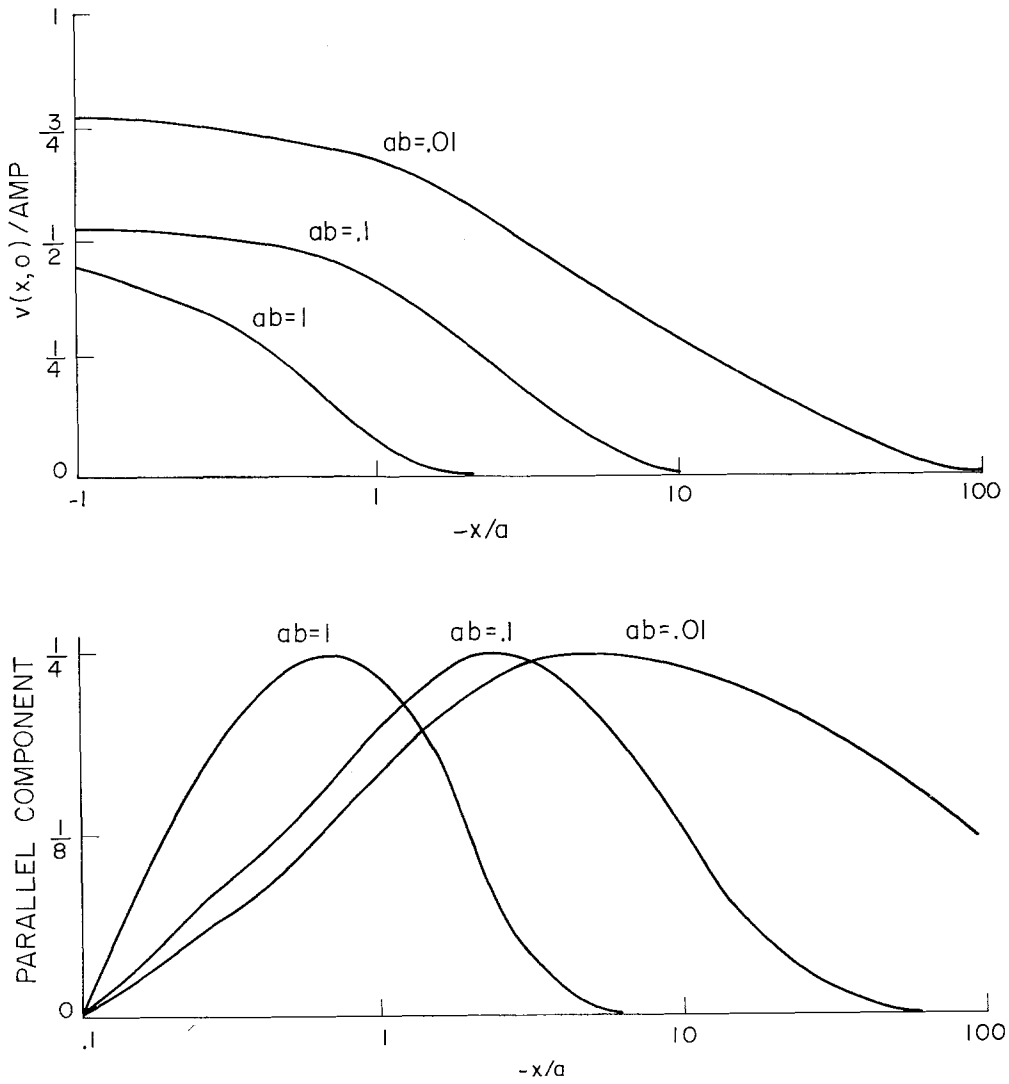

FIG. 7. The components of motion along the fault surface as given by equations (21) and (24).

EFFECT OF RUPTURE VELOCITY AND POISSON'S RATIO

As pointed out earlier, the effect of the velocities on the amplitude of the perpendicular component of displacement along the fault is contained in equation (7). This dependence is illustrated in Figure 9 for a wide range of Mach numbers (V/β) and shear-compressional velocity ratios (or equivalently, Poisson's ratio). The effect of an increase in either quantity is to increase the amplitude of the perpendicular component. Weertman (1969) has pointed out that at the Rayleigh velocity, given by $\gamma_1\gamma_2 = \chi^4$,

the shear stress across the dislocation surface vanishes, and beyond this velocity the shear stress changes sign. This suggests that the Rayleigh velocity may play an important role in the dynamics of moving dislocations. This importance is not, however, indicated in the amplitude function shown in Figure 9. There the obvious characteristic rupture velocity is the shear velocity, at which point the perpendicular displacement diverges to infinity.

It is important to realize that the dependence of the amplitude of the perpendicular displacement on the velocities is *completely* expressed by equation (7) only if the parallel component of motion does not change with rupture velocity. Since most forms of the

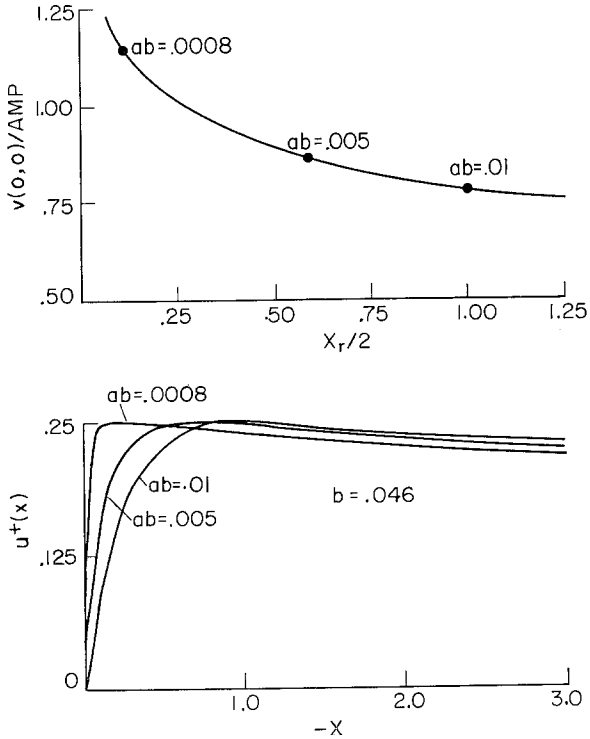

FIG. 8. *Upper*, the influence of the rise-distance, x_r, on the peak amplitude of the perpendicular component. *Lower*, a few examples of the corresponding parallel components. The parameter b was fixed at $b = 0.046$ (this gives $x_r = 2$ when $ab = 0.01$).

parallel component can be characterized by a rise-distance x_r related to rise-time t_r by

$$x_r = Vt_r, \tag{26}$$

this implies that as the rupture velocity increases t_r must decrease in order to keep x_r constant. If, on the other hand, we wish to determine the influence of rupture velocity on a fault model with constant rise-time, we must also take into account the effect of the changing rise-distance in the moving frame. This dependence is shown in Figure 8 for a particular form of the dislocation across the fault surface.

For points away from the fault, it is no longer possible to separate the spatial and material property dependence. In general, the effects of the rupture velocity and Poisson's ratio are to produce relativistic transformations of the y-coordinate, and to

determine the relative proportions of the shear and compressional solutions in the total motion.

As a final point, if two-component near-field measurements are available, the parallel component could be used to obtain directly the total dislocation across the fault surface and the perpendicular component of motion could be used, with the aid of the results in this section, to estimate the rupture velocity.

Application to Parkfield Earthquake

The now famous Parkfield earthquake of June 28 1966 presents one of the few possibilities, up to the present time, of testing our model against actual observations.

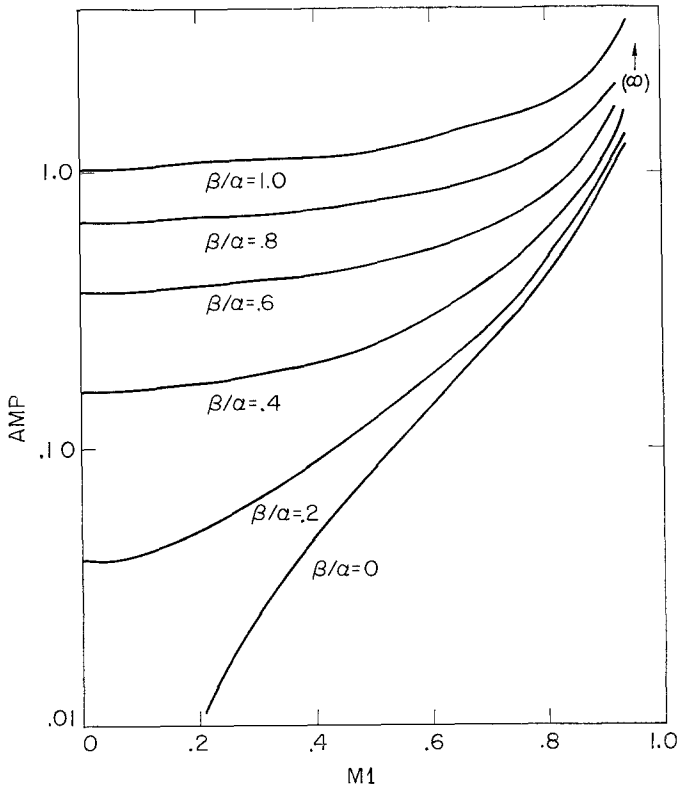

FIG. 9. The behavior of the amplitude factor as defined by equation (7). $M1$ is the shear-wave Mach number V/β.

This earthquake was recorded by a three-component strong-motion seismograph and also by a seismoscope, both located only a short distance from the fault (Housner and Trifunac, 1967). The parallel component of the accelerometer was inoperative at the time of the earthquake, and, thus, most of the discussion below will deal with the perpendicular component. Trifunac and Hudson (1970), however, were able to combine the existing accelerometer traces with the seismoscope record to compute the first few seconds of the parallel acceleration trace. At the end of this section, a rough comparison of the displacement implied by this motion will be made with the dislocation model.

Aki (1968) used the perpendicular displacement, with a peak amplitude of about 30 cm, to estimate the total dislocation produced by the fault. He found this to be approximately 60 cm, whereas the slip across the fault surface observed at the surface of

the ground some time after the event was an order of magnitude smaller. Results in a general study of the elastic fields near a propagating fault by Haskell (1969) imply a dislocation of 95 to 140 cm for this earthquake. In this section we will compare results obtained from the two-dimensional dislocation theory with these more exact estimates. In so doing, we will follow Aki and use the following parameters: $\alpha = 6.0$ km/sec, $\beta = 3.5$ km/sec, $V = 2.2$ km/sec.

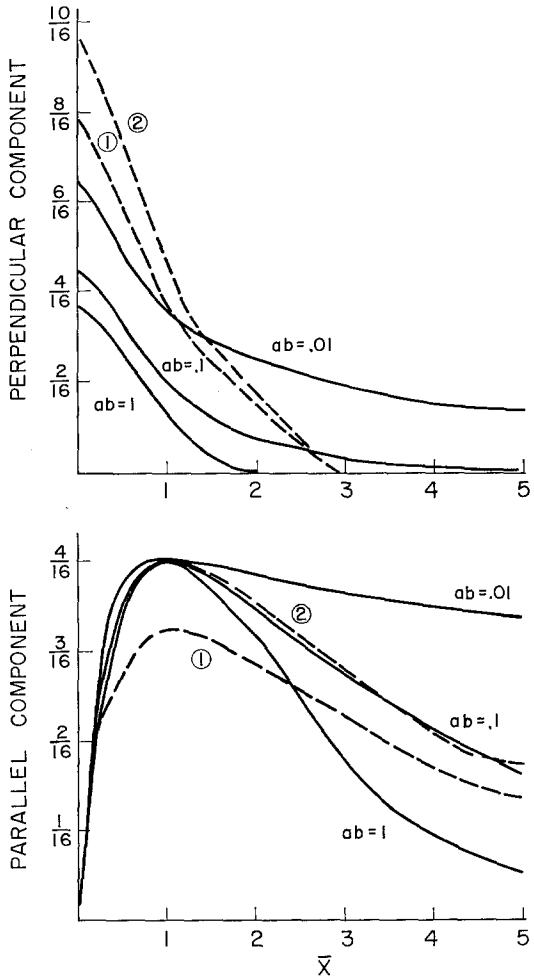

FIG. 10. *Solid lines*, components of motion from Figure 7 with the parameter a chosen such that the peak parallel motion occurs at the normalized distance $\bar{x} = 1$. The velocity ratios shown in Table 1 under Aki have been used in the computation of the perpendicular displacement. *Dashed lines* ①, values of the motion as computed by Aki (1968) taken from his Figure 12 and plotted against the normalized $\bar{x}$. *Dashed line* ②, the motion in ① normalized such that the peak parallel displacement is $d/4$, as required by the boundary condition.

As we have previously noted, the motion shown in Figures 5 and 7 is qualitatively similar to that derived by Aki (1968, Figure 12 in his paper). In order to effect a quantitative comparison we replot the data in Figure 7 by choosing a value of "a" such that the peak in the parallel component occurs at $x = 1$. The resulting motions are shown in Figure 10. The case $ab = 0.1$ is very similar to the motion in Figure 5, which was derived from equation (19). Also shown are Aki's results, again normalized so that the peak in u occurs at $x = 1$.

In plotting Aki's results, an attempt has been made to compensate for the fact that his motions were not calculated on the fault. From his results, calculated at $y = -0.08$ km, we find a zero-to-peak distance in the parallel component of about 0.66 km. Remembering the antisymmetry of u, we note that the zero-to-peak distance is one-half of the rise-distance. Because of the similarity between his results and those derived from equations (19), we can use the data in Figure 6 to show that the zero-to-peak distance at the fault surface would be about 0.53 km, and $u(-0.08)/u(0.0) = 0.82$, $v(-0.08)/v(0.0) = 1.06$. These factors have been applied to his results. Also shown in Figure 10 is the perpendicular component of motion derived by Aki if the parallel component had attained a maximum zero-to-peak amplitude of $d/4$, as required by the boundary condition along the fault.

We see from Figure 10 that although the parallel components derived by Aki and the two-dimensional theory agree quite well, the perpendicular components do not. If, based on the agreement in the parallel component between his results and those for $ab = 0.1$, we estimate d from the two-dimensional results, we get $d \cong 100$ cm. The discrepancy between the results may be partly due to the arbitrary extrapolation of the

TABLE 1

FAULT PARAMETERS

	Aki	Haskell
β/α	0.58	0.58
V/β	0.63	0.77
X_r*	1.0 km	2.0 km
L†	7.0 km	20.0 km
H†	6.0 km	5.0 km

* Approximate distance in moving frame required for total parallel dislocation to be reached.

† See Figure 1. L in Aki's case could be increased without altering the solution in any significant way.

spectra Aki made for very low frequencies. The peak of the perpendicular displacement may not depend strongly on the extrapolation of its spectra, and, thus, we could say that, as far as the peak amplitude is concerned, the perpendicular displacement actually corresponds to a different parallel component of motion from that shown in his Figure 12; the function u^+ to which v does correspond probably has a tail which decreases less rapidly with distance than is shown. Thus, perhaps we should use the results for $ab = 0.01$ rather than 0.1, in which case $d \cong 70$ cm. In any case, some discrepancy should be expected between the three-dimensional and two-dimensional calculations.

We now turn to a comparison with Haskell's results (1969). As opposed to Aki, Haskell derived expressions for the motion by integrating a time-domain Green's function over the fault surface, and, thus, did not have to extrapolate spectral values. He did not, however, base his calculations on a model of the Parkfield earthquake. Even so, one of his models was close enough to that at Parkfield to permit comparison of his theoretical values with the observations. Table 1 contains a comparison between this model and Aki's. If we take Haskell's results for the peak motion at various distances from the fault, as shown in Figures 8.1 and 8.4 in his paper, we can extrapolate the peak motions to the fault (Figure 11). The extrapolation of the parallel component gives a value of $d/2$ units for the offset of a given side of the fault, and, for the perpendicular component, we get $0.2d$ to $0.3d$, depending on the manner of extrapolation. The

leveling off of the perpendicular component shown in Figure 6 would argue for the lower value. The resulting derived total-fault offset, based on an observed perpendicular motion of 30 cm, at 0.08 km from the fault, is then 95 to 140 cm. Actually, as seen in Table 1, Haskell used a higher Mach number than we did in the computations. The results in Figure 9 imply that, if he had used a smaller number, the derived fault offset would have been even larger. On the other hand, Haskell's rise-distance is larger than Aki's. This factor alone would lead to a discrepancy between the derived fault offsets of Aki and Haskell which is similar in sense to that found. The results in Figure 8, however, imply that this factor would, at the most, cancel the effect of the different Mach numbers. Furthermore, if we use Aki's results with the parallel component normalized to $d/4$, or if Aki had used a constant amount of dislocation over the fault surface rather than a dislocation which decreased with depth, we would get a smaller offset than the derived one of 60 cm. It thus seems that a discrepancy exists between

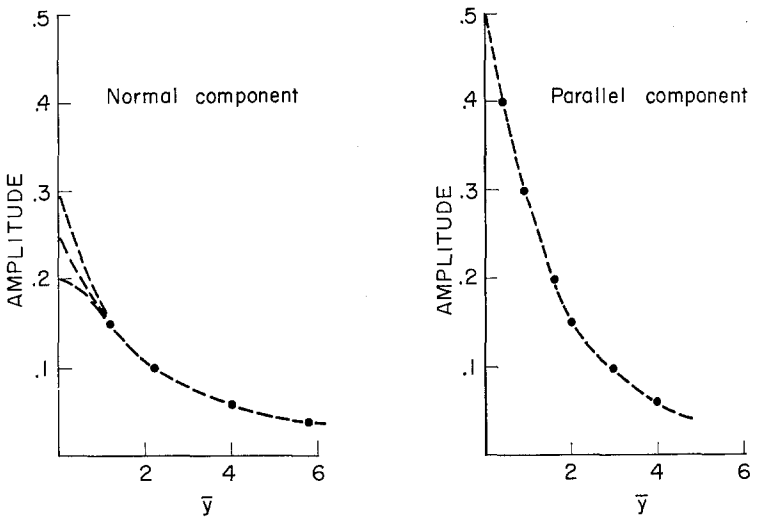

FIG. 11. The *solid dots* are peak values of the motion computed by Haskell (1969). The y-coordinate has been normalized by $V \cdot t_r$ where t_r is the rise-time of a ramp function. Data taken from the middle of the fault surface in Haskell's Figures 8.1 and 8.4. The *dashed lines* are possible extrapolations.

Aki's and Haskell's results. The origin of this discrepancy is not clear, but it is encouraging that the two-dimensional dislocation results fall between their estimates. At any rate, all three of the estimates clearly indicate that the actual fault offset was much larger than observed at the surface.

A rough comparison can also be made with the partial parallel-component acceleration trace derived by Trifunac and Hudson (1970, Figure 6). Disregarding the high-frequency oscillations, which must be due to inhomogeneities of fault motion or material properties, we can fit the function

$$-Ae^{at\,\mathrm{sgn}(t)}\,\mathrm{sgn}\,(t)$$

to the motion, where $A \approx 350$ cm/sec^2, $a \approx 3.3$ sec^{-1}, and the time origin is placed at the obvious jump in acceleration. Upon integrating twice, we find that the displacement has a finite offset of $2A/a^2 \approx 70$ cm, and it is in the proper direction for right lateral motion. Considering that the total offset should be one-half of the total

fault dislocation, we come out with $d \approx 140$ cm. If we define the rise-time as $2/a$, we find it to be 0.6 secs, a value consistent with other reported values. We must not take these deductions very seriously, since they are based on an incomplete time series, but they do show that the parallel component is consistent with the perpendicular component and with the two-dimensional dislocation model.

Discussion

We have shown that the study of two-dimensional gliding-edge dislocations can provide some useful insights into the near-field motion of propagating faults. The use of such dislocations is strictly limited to idealizations of propagating, vertical strike-slip faults which extend to the Earth's surface. Within this context, the dislocation model provides results, for the near-field motions, comparable to those from the more detailed studies of Aki (1968) and Haskell (1969) but with greatly reduced effort and expense.

The simplified fault model we have discussed may be sufficient for a uniform half-space, but is no substitute for the much more complicated and potentially very interesting model of fault propagation is a layered Earth. In particular, the influence on the near-field motions of a layer of low-velocity sediments may be extreme. The effects could range from a decoupling, as discussed by Aki (1968), to a large amplification of the motions. It is also conceivable that a fault propagating subsonically in the lower medium could give rise to supersonic bow waves in the low-velocity sediments. These shock-waves could be very destructive and deserve further study.

Finally, we note that, within the framework presented in this paper, the motion near a propagating tensile crack can be modeled by a uniformly-moving climbing-edge dislocation.

Acknowledgments

Discussions with Raul Madariaga cleared away a few cobwebs existing in the initial draft of this paper.

This research was supported by the Advanced Research Projects Agency, monitored by the Air Force Office of Scientific Research under contract AF 49(638)-1763 and by the National Science Foundation under Grant GA-4039.

References

Aki, K. (1968). Seismic displacements near a fault, *J. Geophys. Res.* **73**, 5359–5376.

Erdélyi, A., Editor (1954). *Tables of integral transforms*, vols. 1 and 2, McGraw-Hill, New York.

Eshelby, J. D. (1949). Uniformly moving dislocations, *Proc. Phys. Soc. (London)* **A62**, 307–314.

Fung, Y. C. (1965). *Foundations of Solid Mechanics*, Prentice-Hall, Englewood Cliffs, N. J.

Futterman, W. I. (1962). Dispersive body waves, *J. Geophys. Res.* **67**, 5279–5291.

Gautschi, W. and W. F. Cahill (1965). Exponential integral and related functions, in *Handbook of Mathematical Functions*, Abramowitz and Stegen, Editors, Dover Publications, Inc., N. Y.

Haskell, N. A. (1964). Total energy and energy spectral density of elastic wave radiation from propagating faults, *Bull. Seism. Soc. Am.* **54**, 1811–1841.

Haskell, N. A. (1969). Elastic displacements in the near-field of a propagating fault, *Bull. Seism. Soc. Am.* **59**, 865–908.

Housner, G. W., and M. D. Trifunac (1967). Analysis of accelerograms—Parkfield earthquake, *Bull. Seism. Soc. Am.* **57**, 1193–1220.

Lamb, G. L., Jr. (1962). The attenuation of waves in a dispersive medium, *J. Geophys. Res.* **67**, 5273–5277.

Savage, J. C. (1965). The stopping phase on seismograms, *Bull. Seism. Soc. Am.* **55**, 47–58.

Titchmarsh, E. C. (1948). *Introduction to the theory of Fourier integrals*, Oxford University Press, London.

Trifunac, M. D., and D. E. Hudson (1970). Analysis of the station no. 2 seismoscope record—1966, Parkfield, California, earthquake, *Bull. Seism. Soc. Am.*, **60**, 785–794.

Weertman, J. (1969). Dislocations in uniform motion on slip or climb planes having periodic force laws, in *Mathematical Theory of Dislocations*, T. Mura, Editor, Amer. Soc. Mech. Engrs., 178–202.

Weertman, J. and J. R. Weertman (1964). *Elementary dislocation theory*, Macmillan Co., New York.

Department of Earth and Planetary Sciences
Massachusetts Institute of Technology
Cambridge, Massachusetts 02139

Manuscript received August 10 1970